**Key Points:**

- The position of the Io, Europa and Ganymede footprints based on Juno-JIRAM observations are reported with unprecedented spatial resolution
- The positions of the footprints support the Juno-based magnetic field models and the calibration of ground-based observation
- The transversal shift of the Ganymede footprint suggests variations of the plasmadisk; the shift appears to be correlated with local time

# The Infrared Auroral Footprint Tracks of Io, Europa and Ganymede at Jupiter Observed by Juno-JIRAM

A. Moirano[1,2] , A. Mura[1] , V. Hue[3,4] , B. Bonfond[5,6] , L. A. Head[5,6] , J. E. P. Connerney[7] , A. Adriani[1] , F. Altieri[1] , C. Castagnoli[1,8,9] , A. Cicchetti[1] , B. M. Dinelli[8] , D. Grassi[1] , A. Migliorini[1] , M. L. Moriconi[1] , R. Noschese[1] , G. Piccioni[1] , C. Plainaki[10] , P. Scarica[1] , G. Sindoni[10] , R. Sordini[1] , F. Tosi[1] , D. Turrini[1] , and F. Zambon[1]

[1]Institute for Space Astrophysics and Planetology, National Institute for Astrophysics (INAF—IAPS), Rome, Italy, [2]Sapienza University of Rome, Rome, Italy, [3]Aix-Marseille Université, CNRS, CNES, Institut Origines, LAM, Marseille, France, [4]Southwest Research Institute, San Antonio, TX, USA, [5]Laboratory for Planetary and Atmospheric Physics, Space Science, Technologies and Astrophysical Research Institute, University of Liège, Liège, Belgium, [6]Space Sciences, Technologies and Astrophysics Research Institute, Université de Liège, Liège, Belgium, [7]Space Research Corporation, Annapolis, MD, USA, [8]Institute of Atmospheric Sciences and Climate, National Research Council (CNR - ISAC), Bologna, Italy, [9]University of Rome Tor Vergata, Rome, Italy, [10]Italian Space Agency (ASI), Rome, Italy

**Abstract** The electromagnetic coupling between the Galilean satellites at Jupiter and the planetary ionosphere generates an auroral *footprint*, which is detected with high spatial resolution in the infrared L band by the Jovian InfraRed Auroral Mapper (JIRAM) onboard the Juno spacecraft. We report the JIRAM data acquired since 27 August 2016 until 23 May 2022, which are used to compute the average position of the footprint tracks of Io, Europa and Ganymede. The result of the present analysis help to test the reliability of magnetic field models, to calibrate ground-based observations and to highlight the variability in the footprint positions, which can be used to probe the plasma environment at the orbit of the satellites. The determination of the plasma properties around the moons is particularly relevant to complement the Juno flybys of the moons during its extended mission, and to support the future Juice and Europa Clipper missions. Lastly, we report no clear evidence of the auroral footprint of Callisto, which is likely due to a combination of its low expected brightness and its position very close to the main Jovian aurora.

**Plain Language Summary** The Jovian InfraRed Auroral Mapper onboard the Juno spacecraft around Jupiter has now been gathering 6 years of observations. Here, we report the position of the auroral infrared emission associated with the orbital motion of Io, Europa and Ganymede. The position of this emission - called *footprint* - carries information on the magnetic field geometry and the distribution of charged particles along the magnetic field. Therefore, the footprint tracks provided here can be used to test and constrain magnetic field models, and to improve the calibration of ground based observations of Jupiter: this can help better understand the source region of the main Jovian aurora and its variations. Lastly, by surveying the data acquired over 40 Juno orbits, we point out variations in the footprint position, which reflect the variability in the plasma conditions near the moons: this monitoring may help determine the mass loading of the magnetosphere, which affects the intensity of the main aurora. The possibility of investigating the plasma environment at the orbit of the satellites is important to complement the satellite flybys performed during the extended mission of Juno and to support the future Juice and Europa Clipper missions, which are dedicated to the Galilean moons.

## 1. Introduction

Jupiter hosts the most intense auroral activity in the Solar System (Grodent, 2015), and its complex morphology can be observed at a variety of different wavelengths, from radio to X-ray (Drossart et al., 1989; Gladstone et al., 2002, 2007; Grodent et al., 2006; Kurth et al., 2017; Trafton et al., 1989). Among the auroral features, the *satellite footprints* are emissions that can be observed at the base of the magnetic shells connected to the orbits of the Galilean moons. The footprint of Io (IFP) was the first to be observed (Clarke et al., 1996; Connerney et al., 1993; Prangé et al., 1996), followed by the Europa and Ganymede footprints (EFP and GFP, respectively) (Clarke et al., 2002) and then that of Callisto (Bhattacharyya et al., 2018). The footprints originate from the relative velocity between each moon and its surrounding plasma (Neubauer, 1980; Saur, 2004): the local perturbation at the moons excites Alfvén waves that propagate along the magnetic field lines (Acuña et al., 1981; Belcher et al., 1981; Neubauer, 1980) at a speed $v_A = B/\sqrt{\mu_0 \rho}$ ($B$ is the magnetic field magnitude and $\rho$ the

plasma mass density). $v_A$ is a few hundred km/s near the moons (Kivelson et al., 2004) and approaches the speed of light in the high-latitude magnetosphere (Hinton et al., 2019). Hence, the wavefronts form a wing-shaped structure in the satellite frame, called an *Alfvén wing* (Drell et al., 1965). The Alfvén waves can exchange energy by wave-particle interaction with magnetospheric electrons (Damiano et al., 2019; Hess, Delamere, et al., 2010; Jones & Su, 2008; Sulaiman et al., 2020), which then precipitate onto the planetary ionosphere. The ionization of the atmospheric hydrogen caused by the electron precipitation forms $H_3^+$, whose infrared (IR) emission can be observed at the satellite auroral footprints (Miller et al., 2020).

In this work, we focus on the emission at the foot of the Alfvén wings, which is called the *Main Alfvén Wing* (MAW) spot (Bonfond et al., 2008). Additionally, we survey the position of the *footprint tails* downstream of the MAW spot (Bonfond et al., 2017), to be compared with the MAW spot position. The position of the MAW spot depends on System III longitude of the moons in Jupiter's frame (from here on, longitudes are tacitly referred in System III). The fast Jovian rotation confines the magnetospheric plasma in a few $R_J$-thick disk around the *centrifugal equator*, which is located ∼7° from the *rotational equator* (Hill, 1979; Moirano, Gomez Casajus, et al., 2021; Phipps et al., 2020). The Galilean moons wiggle up and down in this plasmadisk as they orbit Jupiter: this affects the pattern of the Alfvén wings, thus determining the position of the MAW spot.

Since 2016, the Juno spacecraft has been orbiting Jupiter in a polar orbit (Bagenal et al., 2017; Connerney et al., 2017). The Juno-JIRAM instrument has an L-band imager designed to detect the IR emission from the auroral $H_3^+$, which is produced by the reaction between the molecular hydrogen of the atmosphere and the precipitating electrons (Miller et al., 2020). The high spatial resolution of the instrument allows us to resolve the morphology of the footprints with unprecedented detail (Moirano, Mura, et al., 2021; Mura et al., 2017, 2018). Here, we report all the observations of the Io, Europa and Ganymede footprints performed by Jovian InfraRed Auroral Mapper (JIRAM) from the first perijove (PJ) on 27 August 2016 until PJ42 on 23 May 2022. At present, we find no clear evidence of the Callisto footprint in the JIRAM data set due to the presence of the main auroral emission of Jupiter close to its expected position. Hence, Callisto will be left out of this work.

The main goal of the present work is to provide a survey of all the observations performed by Juno-JIRAM and the reference tracks of the Io, Europa and Ganymede IR footprints, since these observations are the highest resolution images ever made of the auroral footprints. The results will help to test the reliability of magnetic field models by comparing JIRAM observations with their modeled position. Furthermore, the MAW spot can be a reference for calibrating ground-based observations: this will help to better determine the position of the aurorae observed from near Earth, hence improving the quality of the analysis based on those data. Lastly, the JIRAM survey can be used to study the variability of the plasma environment at the orbit of the Galilean satellites (Moirano et al., 2023), as the position of the footprints depends on both the magnetic field and the plasma distribution along the magnetic field lines. The possibility of investigating the plasma parameters near the moons by looking at the footprint is an important tool for complementing the *in-situ* particle measurements that Juno is performing during the flybys of the satellites. The information on the plasma condition and its variability around Europa and Ganymede are fundamental to support the future orbiter mission of Juice and Europa Clipper to the Jovian moons.

## 2. Observations, Data Reduction and Fitting Procedure

The JIRAM L-band imager is a 128 × 432 pixels detector operating between 3.3 and 3.6 μm and with an angular resolution of about 0.01° (Adriani et al., 2017), which corresponds to a few tens of kilometers at the 1 bar level in the Jovian atmosphere (considered the "surface" of Jupiter, which is given by an oblate ellipsoid with equatorial radius $R_J = 71,492$ km and polar radius $R_p = 66,854$ km). Due to the interference from the adjacent M-filter, the data are corrected according to Mura et al. (2017) and the first 38 rows near the M-filter removed.

We survey the observations performed since PJ1 on 27 August 2016 until PJ42 on 23 May 2022. To determine the position of the emissions, we used a 2D peak-finder routine (Natan, 2021). For the MAW spots, we gathered 259 images for Io, 127 for Europa and 234 for Ganymede. This initial data set was then reduced to account for batches of images that show the same MAW spot in the same sequence. Indeed, thanks to the high resolution of JIRAM, these batches do not significantly improve the determination of the footprint position with respect to a single image, but they statistically affect the result of the fitting procedure. Hence, the data points from a single sequence were binned in 500-km-wide bins, and the final data set includes 115 data points for Io), 55 for Europa and 83 for Ganymede. To obtain the tail position, we used *sequences* - that is, tessellations of several images acquired 30 s

**Table 1**
*Summary of the Data set Used in This Work, the Footprint Characteristics (Size and Lead Angle) and the Performance of the Reference Footprint Track Obtained From Jovian InfraRed Auroral Mapper Data set*

|  | Io | Europa | Ganymede |
|---|---|---|---|
| **Data set (Section 2)** | | | |
| MAW - north[a] | 130(56) | 54(17) | 95(32) |
| MAW - south[a] | 129(59) | 73(38) | 139(51) |
| Tail - north[b] | 57 | 13 | 18 |
| Tail - south[b] | 113 | 45 | 47 |
| **MAW spot size (km) (Section 2)** | | | |
| Longitudinal | $438 \pm 156$ | $538 \pm 206$ | $958 \pm 120$ |
| Transversal | $154 \pm 16$ | $202 \pm 24$ | $200 \pm 42$ |
| Vertical | $382 \pm 76$ | $502 \pm 360$ | (400)[c] |
| **Fit residuals (km) (Section 3)** | | | |
| MAW - north | 198 | 65 | 110 |
| MAW - south | 109 | 85 | 293 |
| Tail - north | 231 | 62 | 190 |
| Tail - south | 252 | 150 | 301 |
| **JRM33 residuals (km) (Section 4.1)** | | | |
| ord. 13th | 512(424) | 449(549) | 609(881) |
| ord. 18th | 484(451) | 320(325) | 441(600) |
| **Lead angle (deg) (Section 4.2)** | | | |
| north | $4.2 \pm 2.4(0.1)$ | $6.2 \pm 2.5(0.6)$ | $13 \pm 6(1)$ |
| south | $4.1 \pm 2.0(0.1)$ | $5.7 \pm 3.0(0.4)$ | $11.9 \pm 3.5(0.4)$ |

*Note.* The manuscript reference sections are reported in the first column. For the lead angle: the uncertainty represent the variation due to the wiggling of the moon in the centrifugal frame, while the parentheses contain the accuracy. [a]Number of single images, in format: total(used). [b]Number of sequences. [c]Estimated.

apart - instead of single images. The Io footprint tail (IFPT) was observed in 170 sequences, and the Europa and Ganymede footprint tails (EFPT and GFPT) in 58 and 65, respectively. The number of observations of the MAW spots and the footprint tails from JIRAM are summarized in Table 1.

The coordinates of the MAW spot and the footprint-tail positions are computed at an altitude of $600 \pm 100$ km above the Jovian surface, estimated by stereoscopy of PJ4 and PJ7, when JIRAM observed the IFP between 90° and 120° in the northern hemisphere with two different emission angles of ~75° and ~35° respectively (this is the angle between the normal to the planetary surface and the instrument line of sight). This broadly agrees with the observed peak emission altitude of the main aurora at ~650 km, which has been derived from fundamental emission lines by Kita et al. (2018). It also aligns with the estimated location of the Io spot peak emission from overtone $H_3^+$ emission, placed between 300 and 800 km by Kedziora-Chudczer et al. (2017). According to chemistry models (Tao et al., 2011), the IR emission peaks between 500 and 1,000 km for precipitating electrons with energy between 0.1 and 100 keV. The Juno-JADE-E particle detector (McComas et al., 2017) measured the energy of the precipitating electrons associated with Io (Sulaiman et al., 2020; Szalay et al., 2020b), Europa (Allegrini et al., 2020) and Ganymede (Szalay et al., 2020a). The energy distribution associated with each moon shows remarkable similarity with each other, with a broadband spectrum and the bulk of electrons at energy <1 keV. Because of the above-mentioned Juno observations, the weak dependency of the peak altitude with the precipitating electron energy estimated from the auroral emission model by Tao et al. (2011), and the ground-based observations by Kita et al. (2018) and Kedziora-Chudczer et al. (2017), we conclude that the IR emission of both the MAW spots and the footprint tails of all three satellite is expected to occur between 500 and 700 km. As Juno flies over the Jovian poles, the JIRAM observations are usually performed at small emission angles (i.e., the emission is observed nearly from on top), hence the latitude and longitude of the footprint used in the present work are little sensitive to the precise determination of the altitude of the peak emission. Moreover, observations acquired at high emission angles have large uncertainties (see Equation 4), which corresponds to a smaller weight in the fitting procedure described below: the results of Section 3 are thus little affected by the altitude of the emission.

The positions of the two features are fitted by a Fourier expansion to determine their reference tracks. The fit is performed for each feature (MAW spot or tail) of each moon at both hemispheres separately. For each fit, the best value for the Fourier degree is estimated by computing the mean weighted sum of squared residuals as function of the Fourier degree, that is:

$$MWSSR(N) = \sqrt{\frac{\sum_i W_i D_i^2}{L - (2N+1)}} \qquad (1)$$

where $D_i$ is the $i$th residual (i.e.,: the distance between the $i$th data point and the fitted curve), $W_i$ its normalized weight, $L$ the number of observations and $N$ the degree of the Fourier expansion. The weights in Equation 1 are obtained from

$$w_i = \frac{1}{\Delta_x^2 + \Delta_y^2 + \Delta_z^2} \qquad (2)$$

and their normalization

$$W_i = \frac{w_i}{\sum_i w_i} \tag{3}$$

The denominator of Equation 2 represents the uncertainty on the position of the MAW and footprint tail positions, which includes three contributions: (a) the uncertainty on the altitude of the emission, (b) the physical size of the MAW spot/tail and (c) the resolution of the image. The uncertainty $\Delta_k$ ($k$ being an $xyz$ coordinate) on the position of the MAW spots is then computed as

$$\Delta_k = \sqrt{\Delta_{h(k)}^2 + \Delta_{size(k)}^2 + \Delta_{res(k)}^2} \tag{4}$$

where the three term on the rhs are the above-mentioned source of uncertainty. The uncertainty $\Delta_{h(k)}$ is computed by using the instrument pointing provided by the Navigation and Ancillary Information Facility (NAIF; C. H. Acton, 1996; C. Acton et al., 2018) and by referencing the images at surfaces at the different altitudes of $600 \pm 100$ km. The longitudinal and transversal size of the MAW spots ($\Delta_{size}$) is estimated from images captured at an emission angles $<15°$, while we selected images at emission angles $>70°$ for the vertical extension. Un-luckily, no images of the GFP at high emission angle are available. Nevertheless, the energy distribution of the precipitating electrons associated with the GFP is similar to the distribution of the EFP and IFP, thus we can assume that the vertical extension of the GFP is also similar to the other two. The longitudinal-transversal-vertical size of the MAW is reported in Table 1. The higher longitudinal size of the GFP is due to the presence of two lobes in the MAW spot, which are potentially caused by the geometry of the intrinsic magnetic field of Ganymede. The uncertainty $\Delta_{size}$ of the footprint tail in Equation 4 takes into account its transversal and vertical extension.

## 3. Results

In panel a and b of Figure 1, we report the position of the MAW spots and the footprint-tail positions respectively, alongside the results of the fitting procedure of Section 2. Each point is color-coded according to its local time (LT) and two palettes were used to highlight any potential indication of LT variations. The best value for the Fourier-expansion degree $N$ was determined to be nine in the north and five in the south. In the remainder of this work, relative distances on the Jovian surface - such as potential model-observation discrepancies or the distance between two features - are usually reported in kilometers. These can be approximately converted into angular distances with the following formula:

$$\Delta r = \sqrt{R_p^2 + \frac{R_J^2 - R_p^2}{1 + \frac{R_J^2}{R_p^2}\tan^2\theta}} \Delta\theta \tag{5}$$

where $\Delta r$ is the distance given in kilometers, $R_J = 71{,}492$ km and $R_p = 66{,}854$ km are the equatorial and polar radii of Jupiter, $\theta$ the average latitude of the two features, and $\Delta\theta$ the angular distance corresponding to $\Delta r$.

In panel (a) of Figure 1, in the north, only about half of each track is sampled by the JIRAM observations. JIRAM was able to observe IFP and GFP at $60°–120°$ and around $140°$ longitude respectively, while there are only a few observations for Europa around $120°$. In this region, we observe deviations between the fit and JRM33+Con2020 up to $\sim1{,}000$ km. Poleward deviations of about $1{,}000$ km between the GFP track and the model can also be noticed at $240°–280°$ longitude. In the southern hemisphere the coverage is almost complete, the largest gap being in the GFP between $0°$ and $40°$ longitude. Between $210°$ and $320°$, the fit to the IFP, EFP and GFP are poleward of JRM33+Con2020 by up to $\sim600$, $\sim400$, and $\sim200$ km, respectively. Between $60°$ and $120°$ longitude, the GFP appears displaced poleward when it is observed in the dusk sector, while it is equatorward in the dawn sector. For each fit, we computed the root mean square (rms) of the residuals $R_{fit} = \sqrt{\sum_i D_i^2 / L}$, which are 198, 65, and 110 km for Io, Europa and Ganymede in the north respectively, and 109, 85, and 293 km in the south.

In panel (b), we report the same plots as in panel (a), but here showing the position of the footprint tails. The data coverage of the IFPT is almost complete and the only gap is around $150°–160°$. This improvement is due to the long extension of the IFPT (Bonfond et al., 2017; Mura et al., 2017, 2018). All the differences between the MAW spot position and JRM33+Con2020 are also observed in the plots of panel (b), as well as the transversal
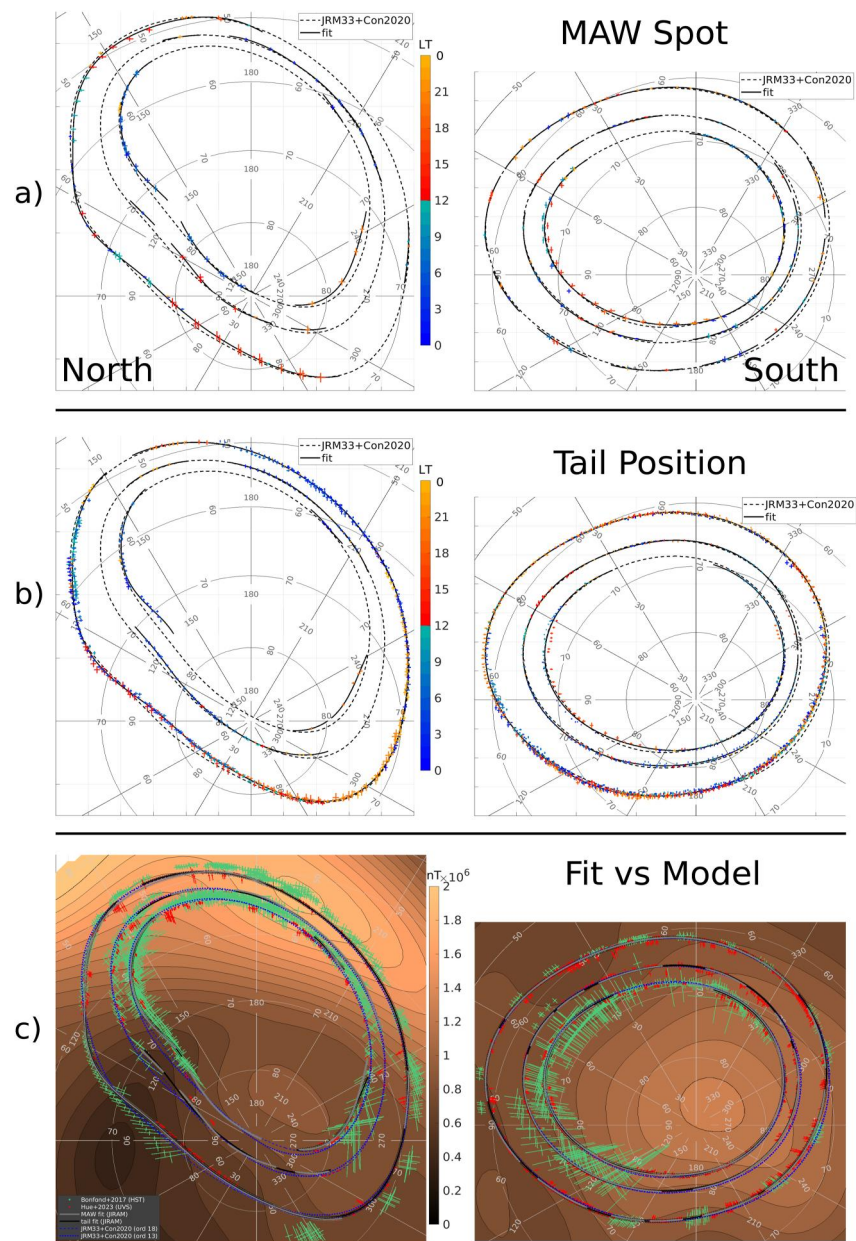
**Figure 1.** (a) Position of the Main Alfvén Wing (MAW) spot of Io, Europa and Ganymede in the north and south (left and right columns, respectively). The data are color-coded according to the local time of the footprint. The gray continuous line is the fit to the data, the gray dashed line is the footprint track predicted by the JRM33+Con2020 magnetic field model. (b) The same as in panel (a), but for the position of the footprint tails. (c) Comparison among the fits obtained from the MAW spots (gray line) and the footprint tails (black line), the JRM33+Con2020 model expanded up to order thirteenth and eighteenth (blue dotted and blue dashed lines, respectively) and the observations performed by the Hubble Space Telescope (green points, from Bonfond et al., 2017) and Juno's ultraviolet spectrograph (red points, from Hue et al., 2023). The gray and black lines are surrounded by thin dotted lines of the same colors: they represent the confidence of the two fits, respectively. The background contours are the magnetic field magnitude at the surface according to JRM33+Con2020 to order eighteenth.

variability of the GFPT between 60° and 120° longitude. The rms of the residuals $R_{fit}$ obtained from the footprint tails are 231, 62, and 190 km for Io, Europa and Ganymede in the north respectively, and 252, 150, and 301 km in the south. The rms of the residuals is also reported in Table 1.

The fitted footprint tracks of panel (a) and (b) are compared in panel (c) and they are largely compatible within the rms of the residuals. Therefore, we suggest that both the MAW spots and the footprint tails can be used

**Figure 2.** *Left*: Lead angles of the Io, Europa and Ganymede Main Alfvén Wing spots in the northern hemisphere. The data are color-coded according the local time. The black line is the fit with a first-order Fourier expansion, the gray shaded area the associated 95% confidence interval. The red dotted line and the red shaded area are the fit to the lea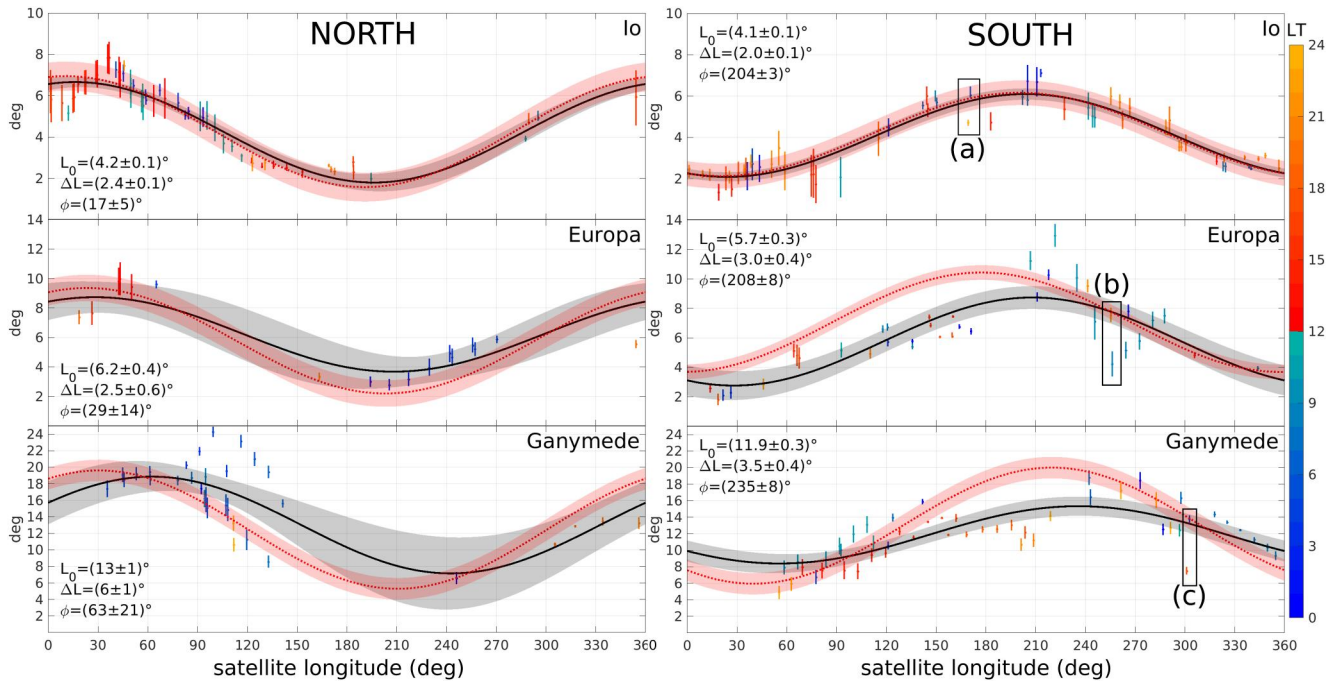d angle derived from Juno's ultraviolet spectrograph observations (Hue et al., 2023). In each plot, we report the parameters obtained by fitting $L_0 + \Delta L \cos(\lambda - \phi)$ to Jovian InfraRed Auroral Mapper data. *Right*: the same as panel on the left, but for the southern hemisphere. The boxes labeled a, b, and c highlight cases of high variability (see also Figure 4).

interchangeably to determine the reference ovals of the footprint tracks. The tables with footprint positions and their reference track shown in Figure 1 can be found in Supporting Information S1 and in Moirano (2023).

To highlight the variability of the position of the footprints, we computed the *lead angle* (Hess, Pétin, et al., 2010; Hue et al., 2023), which is computed by first tracing the MAW spot position along the magnetic field to the equatorial plane and then computing the angular separation with the corresponding moon at the same epoch. This quantity depends on the Alfvén travel time between the satellites and the Jovian ionosphere, so it contains information about the magnetic field and plasma mass distribution in the magnetosphere. In Figure 2, we report the lead angles relative to the observations of Figure 1. The lead angle is fitted with a periodic function $L_0 + \Delta L \cos(\lambda - \phi)$, where $L_0$, $\Delta L$, and $\phi$ are free parameters and $\lambda$ is the longitude of the satellites. The results of these fits are presented alongside the plots of Figure 2 and summarized in Table 1.

## 4. Discussion

### 4.1. Comparison With the JRM33+Con2020 Magnetic Field Model

We computed two predictions by expanding the spherical harmonics of JRM33 up to order thirteenth and eighteenth, which are the recommendations in the original work by Connerney et al. (2022), depending on the level of confidence of the magnetic field coefficients. In panel (c) of Figure 1, the two expansions show differences in the longitude sector between 270° and 170° in the northern hemisphere. Thus, we compare the rms $R_{13}$ and $R_{18}$ of the distance between JIRAM data and the two JRM33+Con2020 predictions in the northern hemisphere (the two expansions lead to very similar footprint tracks in the southern hemisphere). For Io, we obtain $R_{13} = 512$ km and $R_{18} = 484$ km from the MAW spot position and $R_{13} = 424$ km and $R_{18} = 451$ km from the tail position. Indeed, in the longitude sectors 300°–330° and 100°–130°, the order eighteenth better matches the JIRAM data, while the order thirteenth is better between 30° and 100°. Instead, for Europa and Ganymede, $R_{18}$ is smaller than $R_{13}$ for both the MAW spot position and the tail positions. For Europa we obtain $R_{13} = 449$ and 549 km for the two features respectively, and $R_{18} = 320$ and 325 km, while for Ganymede $R_{13} = 609$ and 881 km,
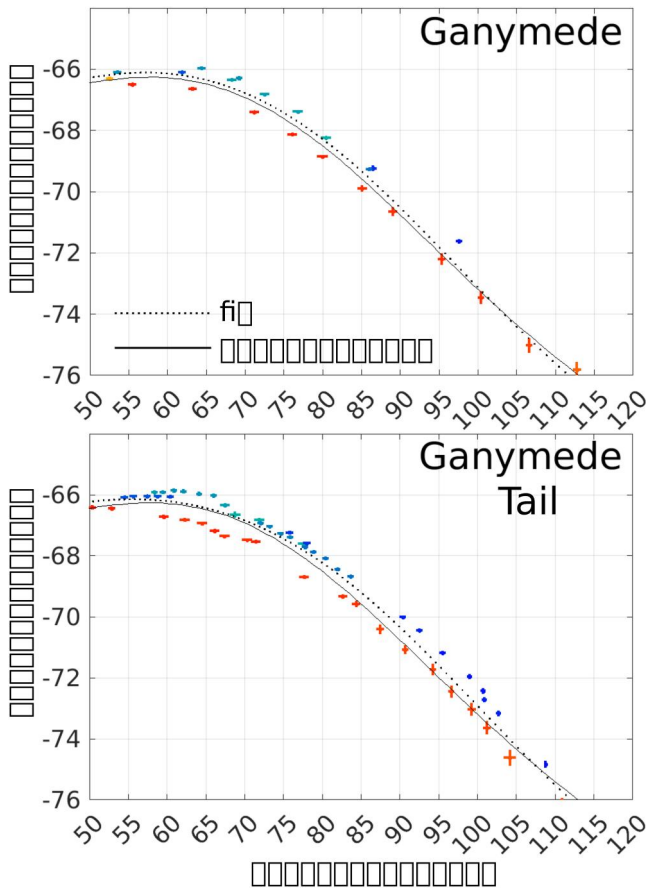
**Figure 3.** Longitude-latitude plot of the position of the Main Alfvén Wing spot (top) and tail (bottom) of the Ganymede footprint. The warm colors represent observations on the dusk sector (points below the dotted line of the fit), the cold colors observations on the dawn sector (point above the fit line). The black line is the prediction based on the JRM33+Con2020 model.

and $R_{18} = 441$ and 600 km. The rms of the difference between the fit based on JIRAM data and the predictions based on JRM33+Con2020 is summarized in Table 1.

According to the residual analysis presented here, we thus suggest expanding the JRM33 spherical harmonics up to order eighteenth for mapping the magnetospheric region from around Europa to Ganymede to the northern hemisphere of Jupiter. For Io, both expansions of JRM33 appear overall equally valid, although the expansion up to order eighteenth should be preferred in the longitude sectors 300°–330° and 100°–130°. For mapping toward the southern hemisphere, there is no preferred choice of the order expansion, as both order thirteenth and eighteenth lead to the same prediction within JIRAM spatial resolution.

### 4.2. Footprint Variability: Lead Angles and Transversal Shift

The position of the MAW spots depends on the shape of the Alfvén wings, which, in turn, are determined by the magnetic field and by the plasma distribution in the magnetosphere. Therefore, in principle, any variation in the position of the MAW spots could be attributed to changes in either the plasma environment and/or the magnetic field.

In Figure 1, the GFP exhibits transversal displacements, which is also reported in Figure 3 for a better view. JIRAM was able to observe the GFP in both hemispheres during PJ1, PJ4, and PJ7; among these, Ganymede orbited in the same longitude sector during both PJ1 and PJ4. These two orbits allowed to sample the GFP track at 140° longitude and 60°–70° latitude north, where no clear evidence of latitudinal displacement is observed. The LT of the northern MAW spot during PJ1 and PJ4 was 4–5 hr and 7–9 hr respectively, thus both observations were in the dawn sector. In the southern hemisphere, the GFP was observed at ∼ −66° latitude, between 70° and 80° longitude during both orbits, showing a latitudinal offset of $0.75 \pm 0.19°$, which corresponds to a transversal displacement of $880 \pm 220$ km. The LT of those observations was 11–12 hr for PJ1 (dawn sector, with the footprint equatorward displaced) and 15 hr for PJ4 (dusk sector, with the footprint poleward displaced). This suggests that the variability of the GFP position

reported here might be due to a local-time asymmetry. Further evidences can be observed in the GFP and the GFPT position in the southern hemisphere at ∼165° longitude, where the emission during PJ25 (LT = 14 hr) was equatorward with respect to PJ21 (LT = 2 hr) and PJ32 (LT = 5 hr) by $0.3 \pm 0.1°$, or $370 \pm 140$ km, and at 310° longitude, where the tail during PJ10 (LT = 19) was poleward with respect to PJ19 (LT = 4) and PJ33 (LT = 12 hr) by about $0.6 \pm 0.3°$, or $660 \pm 330$ km. We also looked for a potential day-night correlation (not shown), but the transversal shift showed no systematic dependency with this criterion. The transversal displacement of the GFP has already been observed by the Hubble Space Telescope (HST; Grodent et al., 2008) and it has been explained by variations in the plasmadisk mass and/or radial transport (Promfu et al., 2022). Although the observations performed during PJ1 and PJ4 suggest local-time variability, we cannot completely rule out a global variation of the plasmadisk. Nevertheless, this change should have occurred over less than 10 hr in order to explain the different north-south displacement observed by JIRAM. Unfortunately, JIRAM did not record the GFP crossing from the dawn to the dusk sector (or vice-versa), which might have represented stronger evidence of its local-time variability.

The lead angle in Figure 2 helps to detect evidence of longitudinal variability between different orbits. In the north, we report a single case for Io at ∼290° between PJ20 and PJ34, and one for Ganymede between 90° and 135°, where the lead angle of PJ1 was larger than the one of PJ4, PJ9, PJ32, and PJ37. In the south, we identified several cases: for Io there is PJ11–PJ32 at 170° longitude; for Europa PJ18–PJ32 at 120°, PJ8–PJ40 at 135°, PJ14–PJ29 at 160°, PJ7–PJ37 at 255° and PJ7–PJ26 at 265°; for Ganymede PJ1–PJ4 between 90° and 120°, PJ4–PJ7 at 160° and PJ30–PJ33 and PJ10–PJ19, both around 300°. For each satellite, we select one example pair of
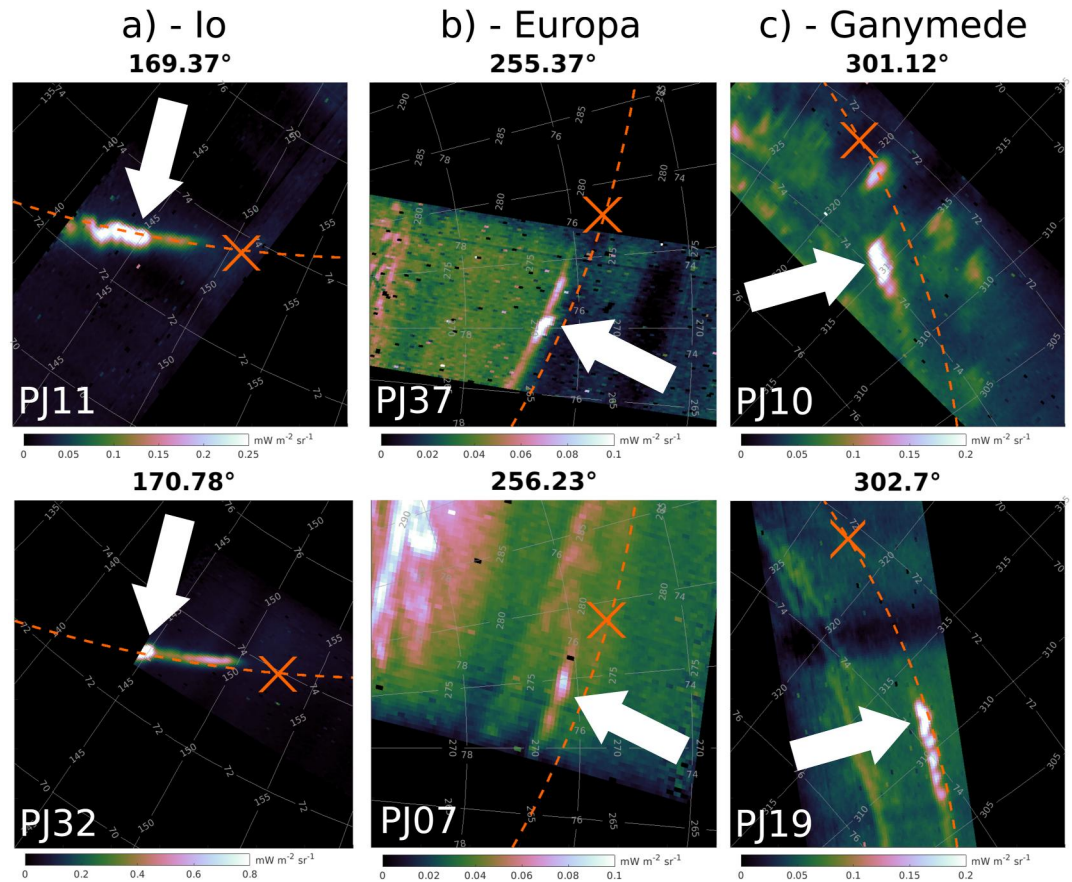
**Figure 4.** Examples of variation in the Main Alfvén Wing (MAW) spot position for Io (left), Europa (center) and Ganymede (right). The orange dashed line is the satellite footprint track according to JRM33+Con2020, the cross is the magnetic footprint of each moon at the time of the acquisition of the image. System III longitude of the satellites is reported above each image. The white arrows point to the MAW spot in each image.

observations, labeled a, b, and c in Figure 2, and reported in Figure 4. Case a shows the IFP during PJ11 and PJ32, with lead angles $4.7 \pm 0.2°$ and $6.0 \pm 0.3°$, respectively. This pair of observations was analyzed in Moirano et al. (2023), where the difference was attributed either to changes in the state of the Io Plasma Torus (Bagenal & Dols, 2020) between the two orbits or to the local-time asymmetry of the plasma torus. Case b shows the longitudinal displacement of the EFP by comparing PJ7 and PJ37, when the lead angle was $4.3 \pm 0.8°$ and $7.5 \pm 0.5°$ respectively, while Europa was at the same longitude within less than 1°. In case c, the GFP exhibits both transversal and longitudinal displacement by comparing PJ10 and PJ19 (lead angle $7.5 \pm 0.5°$ and $13.8 \pm 0.5°$, respectively). The transversal displacement in case c can be ascribed to a LT asymmetry as discussed in the previous paragraph, but we found no clear local-time dependency of the lead angle. A summary of the best-fit values of the lead angle is given in Table 1.

The longitudinal and the transversal displacements of the footprints can be explained by two different processes. The former can be caused by a change in the Alfvén travel time - which corresponds to a variation in the plasma environment - or to a change in the radial current of the plasmadisk - which causes an azimuthal stretch of the magnetic field lines. On the other hand, a transversal displacement can be explained by the satellites connecting to different magnetic shells, which can be due to variations in the azimuthal component of the magnetodisk current that radially stretches the magnetic field. We estimated the longitudinal and transversal displacement by changing the radial current of the Con2020 model $\mu_0 I_R/2\pi$ between 7.7 and 35.2 MA, and the azimuthal current $\mu_0 I_{MD}/2$ between 124.2 and 156.1 nT, according to the Juno magnetometer data (Connerney et al., 2020). The predicted longitudinal shift is approximately 70, 200, and 450 km for Io, Europa and Ganymede respectively, while the transversal shift is about 100, 250, and 650 km. For Io and Europa, these values are similar to or smaller than the footprint size; hence it appears unlikely that the variability observed at those moons is caused by changes in the

plasmadisk currents. Furthermore, both the IFP and EFP exhibited lead angle variations, but no transversal variation, which suggests variations in the plasma environment around the two satellites. On the other hand, the GFP displacement in Figures 1 and 3 may be compatible with magnetodisk variations such as the ones detected by the Juno magnetometer. Thus, we suggest that the variations in the GFP position can be caused either by LT asymmetry and temporal variations of the magnetodisk currents or changes in the plasmadisk mass content.

In summary, the GFP position can exhibit latitudinal shifts, which are suggested to be due to a local-time asymmetry of the magnetosphere. This is supported by the observations at the southern hemisphere, where the GFP has been detected at different latitudes by $0.75 \pm 0.19°$ while being in a different dawn-dusk hemisphere. The same shift was not observed during the same PJs at the northern hemisphere. Moreover, the lead angle associated with Io, Europa and Ganymede shows variability by comparing observation with the satellites at the same System III longitude at different epochs. This implies a variation in the Alfvén travel time, which determines the mapping between the moons and their emission (e.g.,: Hinton et al., 2019; Moirano et al., 2023). This might be caused by either a change in the plasma conditions or a transient longitudinal stretching (or contraction) of the magnetic field, which in turn can be due to variations in the radial plasmadisk currents. Only the GFP position shows latitudinal variations, which may be ascribed to the radial stretching of the magnetic field, caused by changes in the azimuthal plasmadisk currents. The JIRAM observations are in agreement with the magnetodisk currents estimated by the Juno-MAG instrument (Connerney et al., 2020).

### 4.3. Comparison With Juno-UVS and HST Observations

In panel (c) of Figure 1, we compare the fit obtained from the MAW spot and tail positions against the ultraviolet observations performed by HST (Bonfond et al., 2017) and Juno's ultraviolet spectrograph (Juno-UVS; Hue et al., 2023). For the IFP in the north, the HST observations are systematically equatorward with respect to both the JIRAM-based fits and UVS data. In the south, the HST observations usually lie equatorward with respect to the Juno measurements roughly between 30° and 120° longitude, while at the other longitudes the data from the two spacecrafts agree within the HST uncertainty. The HST data of the GFP between 40° and 60° longitude seems to suggest a transversal shift of the GFP of about 2,400 km between September 2009 (poleward) and December 2000, January 2001 and May 2007 (equatorward). We inspected the local-time distribution of these observations, but we found no clear evidence of local-time dependency as in the JIRAM data. Lastly, the lack of observations in the northern hemisphere during September 2009 prevents a north-south comparison of this shift.

The referencing of the HST images onto the Jovian surface is radically different from the one used for Juno. For HST, the inferred position of the footprints relies on the localization of the planetary center, which in turn is determined by fitting the planetary limb in the HST images themselves (Bonfond et al., 2009). On the other hand, Juno-based observations are localized using the spacecraft ephemeris and the instrument pointing, which are provided by the NAIF (C. H. Acton, 1996; C. Acton et al., 2018). Therefore, the different referencing procedures for HST and Juno might be the root cause of the discrepancy among the observations performed by the two spacecrafts. Now, thanks to the fits in Figure 1, it becomes possible to automatically compute the location of Jupiter's center relative to the IFP MAW spot for any HST image in which the Io footprint is visible and use this spot to improve significantly the referencing accuracy. This new method assumes that the location of the MAW spot is stable through time at resolution of HST: both the data shown in Figure 1 and the Io lead angle in Figure 2 suggest that the IFP position varies only occasionally, thus we suggest that its MAW spot is a reliable reference.

The Juno-UVS data in Figure 1 are very consistent with the JIRAM fits. In the north, the UVS observation of the IFP between 60° and 120° longitude performed during PJ8, PJ12, PJ15, and PJ18 matches very well the fits in the same region, which was observed by JIRAM during PJ4, PJ7, PJ15, and PJ18. The UV and IR measurements also agree between 250° and 290° longitude of the GFP, where they both show a poleward displacement with respect to JRM33+Con2020. In the south, UVS data shows the transversal displacement in the GFP at ~75°–90° longitude, where the GFP was displaced poleward during PJ7 (LT = 18 hr) with respect to PJ27 (LT = 8). Unfortunately, no measurements are reported in the northern hemisphere during those PJs for comparison. In Figure 2, the lead angle derived from JIRAM data is compared with the one from UVS data. For Io, the sinusoidal fit to the lead angle appears almost symmetric between the two hemispheres, apart from a phase difference of $187 \pm 8°$, and it matches the result obtained by UVS. The lead angle phases are consistent with the tilt of the centrifugal equator toward ~200° longitude (Moirano, Gomez Casajus, et al., 2021; Phipps et al., 2020) and the wiggling up and down of Io within the Io Plasma Torus. The Europa lead angle is also consistent between the two

hemisphere, the phase difference being ~179 ± 22°. The Europa lead angle is also compatible with the position of the centrifugal equator, showing a maximum at 29 ± 14° in the north and 208 ± 8° in the south. The UVS results shows a larger lead angle than JIRAM, and the phase difference between JIRAM and UVS is about 20° in the south. At Ganymede, the amplitude of the lead angle in the northern hemisphere is larger than the amplitude in the south ($\Delta L = 6 \pm 1°$ and $3.5 \pm 0.4°$, respectively), and the two fits are out of phase by 172 ± 29°. Unlike the Io and Europa lead angles, the Ganymede lead angle peaks at 63 ± 21° in the north and 235 ± 8° in the south, while UVS data reported ~30° and ~220°, respectively. The differences between the JIRAM and UVS lead angles at Europa and Ganymede might be due to the different coverages between the two instrument, combined with the intrinsic variability of these footprints.

To summarize, the ground-based observations of the footprints from HST do not always agree with the reference footprint track derived in the present study. The most probable cause for such discrepancy is the limb-fitting method used to determine Jupiter's location in HST images (Bonfond et al., 2009), which is less accurate than using the instrument pointing from an in-situ spacecraft such as Juno. On the other hand, the footprint positions from Juno-UVS images (Hue et al., 2023) agrees well with the reference track obtained from JIRAM data set. As the processing of JIRAM and UVS data are performed independently, their mutual agreement supports the validity of the reference track shown in Figure 1. Nevertheless, the JIRAM and UVS images shows differences in the footprint lead angle of Europa and Ganymede. This difference between the two data sets might be caused by either the intrinsic variability of the footprint positions or the different coverage of the two instrument. A dedicated analysis would be necessary to further address this question.

## 5. Conclusions

We reported the Juno-JIRAM infrared observation of the Io, Europa and Ganymede auroral footprints observed over 42 spacecraft orbits, between August 2016 and May 2022. The main goal is to provide the reference tracks for the three footprints, which serve a variety of purposes, here summarized:

- The footprint position can be used to test the reliability of magnetic field models. By comparison with the Juno-based magnetic field model JRM33+Con2020 (Connerney et al., 2020, 2022; Wilson et al., 2023), we conclude that the model precisely predict the footprint tracks, although variations up to ~1,000 km are reported between 60° and 140° longitude in the northern hemisphere, as well as deviations up to ~600 km between 210° and 320° longitude in the south. Therefore, we recommend the expansion of the harmonics of the JRM33 internal field up to order eighteenth for the Europa and Ganymede position. For the Io footprint, the expansion up to order eighteenth works better in the longitude sectors 300°–330° and 100°–130°, while we suggest the order thirteenth between 30° and 100°.
- The positions of the MAW spots in JIRAM data agree very well with the Juno-UVS observations, while the positions derived from HST campaigns are occasionally systematically displaced (such as the IFP north). Therefore, we suggest using the reference track reported in the present manuscript to calibrate the localization of ground-based observations, when the MAW spot of the footprint can be identified. Due to the variability of the Ganymede footprint (and of the Europa footprint, to a lesser extent), we recommend using the Io footprint whenever possible.
- The footprint position can be used to investigate the plasma environment near the moons (Moirano et al., 2023) by studying the lead angle associated with the footprints themselves (Hue et al., 2023). For this reason, the footprints represent (a) a source of information that complements the particle measurements carried by Juno during the satellite flybys in its extended mission, and (b) a supporting data set for the next missions Juice and Europa Clipper, which are dedicated to the Jovian major moons.

We also report the transversal shift of the Ganymede footprint by ~900 km (corresponding to ~0.8° in latitude, see Figure 3), which appear to be local-time dependent and it might be explained by variations in the external magnetic field due to the plasmadisk current, that radially stretches the magnetic field.

## Data Availability Statement

JIRAM data and materials used in this study are publicly available on the Plan-etary Data System (Adriani et al., 2019). The repository for the data products used in this study can be found in Moirano (2023).

## References

Acton, C., Bachman, N., Semenov, B., & Wright, E. (2018). A look towards the future in the handling of space science mission geometry. *Planetary and Space Science*, *150*, 9–12. https://doi.org/10.1016/j.pss.2017.02.013

Acton, C. H. (1996). Ancillary data services of NASA's navigation and ancillary information facility. *Planetary and Space Science*, *44*(1), 65–70. https://doi.org/10.1016/0032-0633(95)00107-7

Acuña, M. H., Neubauer, F. M., & Ness, N. F. (1981). Standing Alfvén wave current system at Io: Voyager 1 observations. *Journal of Geophysical Research*, *86*(A10), 8513–8521. https://doi.org/10.1029/JA086iA10p08513

Adriani, A., Filacchione, G., Di Iorio, T., Turrini, D., Noschese, R., Cicchetti, A., et al. (2017). JIRAM, the Jovian infrared auroral mapper. *Space Science Reviews*, *213*(1–4), 393–446. https://doi.org/10.1007/s11214-014-0094-y

Adriani, A., Noschese, R., & Huber, L. (2019). Juno JIRAM bundle [Dataset]. PDS Atmospheres (ATM). https://doi.org/10.17189/1518967

Allegrini, F., Gladstone, G. R., Hue, V., Clark, G., Szalay, J. R., Kurth, W. S., et al. (2020). First report of electron measurements during a Europa footprint tail crossing by Juno. *Geophysical Research Letters*, *47*(18). https://doi.org/10.1029/2020GL089732

Bagenal, F., Adriani, A., Allegrini, F., Bolton, S. J., Bonfond, B., Bunce, E. J., et al. (2017). Magnetospheric science objectives of the Juno mission. *Space Science Reviews*, *213*(1–4), 219–287. https://doi.org/10.1007/s11214-014-0036-8

Bagenal, F., & Dols, V. (2020). The space environment of Io and Europa. *Journal of Geophysical Research: Space Physics*, *125*(5). https://doi.org/10.1029/2019JA027485

Belcher, J. W., Goertz, C. K., Sullivan, J. D., & Acuña, M. H. (1981). Plasma observations of the Alfvén wave generated by Io. *Journal of Geophysical Research*, *86*(A10), 8508–8512. https://doi.org/10.1029/JA086iA10p08508

Bhattacharyya, D., Clarke, J. T., Montgomery, J., Bonfond, B., Gérard, J., & Grodent, D. (2018). Evidence for auroral emissions from Callisto's footprint in HST UV images. *Journal of Geophysical Research: Space Physics*, *123*(1), 364–373. https://doi.org/10.1002/2017JA024791

Bonfond, B., Grodent, D., Gérard, J.-C., Radioti, A., Dols, V., Delamere, P. A., & Clarke, J. T. (2009). The Io UV footprint: Location, inter-spot distances and tail vertical extent. *Journal of Geophysical Research*, *114*(A7). https://doi.org/10.1029/2009JA014312

Bonfond, B., Grodent, D., Gérard, J.-C., Radioti, A., Saur, J., & Jacobsen, S. (2008). UV Io footprint leading spot: A key feature for understanding the UV Io footprint multiplicity? *Geophysical Research Letters*, *35*(5), L05107. https://doi.org/10.1029/2007GL032418

Bonfond, B., Saur, J., Grodent, D., Badman, S. V., Bisikalo, D., Shematovich, V., et al. (2017). The tails of the satellite auroral footprints at Jupiter. *Journal of Geophysical Research: Space Physics*, *122*(8), 7985–7996. https://doi.org/10.1002/2017JA024370

Clarke, J. T., Ajello, J., Ballester, G., Ben Jaffel, L., Connerney, J., Gérard, J.-C., et al. (2002). Ultraviolet emissions from the magnetic footprints of Io, Ganymede and Europa on Jupiter. *Nature*, *415*(6875), 997–1000. https://doi.org/10.1038/415997a

Clarke, J. T., Ballester, G. E., Trauger, J., Evans, R., Connerney, J. E. P., Stapelfeldt, K., et al. (1996). Far-ultraviolet imaging of Jupiter's aurora and the Io "footprint". *Science*, *274*(5286), 404–409. https://doi.org/10.1126/science.274.5286.404

Connerney, J. E. P., Adriani, A., Allegrini, F., Bagenal, F., Bolton, S. J., Bonfond, B., et al. (2017). Jupiter's magnetosphere and aurorae observed by the Juno spacecraft during its first polar orbits. *Science*, *356*(6340), 826–832. https://doi.org/10.1126/science.aam5928

Connerney, J. E. P., Baron, R., Satoh, T., & Owen, T. (1993). Images of excited H3+ at the foot of the Io flux tube in Jupiter's atmosphere. *Science*, *262*(5136), 1035–1038. https://doi.org/10.1126/science.262.5136.1035

Connerney, J. E. P., Timmins, S., Herceg, M., & Joergensen, J. L. (2020). A Jovian magnetodisc model for the Juno era. *Journal of Geophysical Research: Space Physics*, *125*(10), e2020JA028138. https://doi.org/10.1029/2020JA028138

Connerney, J. E. P., Timmins, S., Oliversen, R. J., Espley, J. R., Joergensen, J. L., Kotsiaros, S., et al. (2022). A new model of Jupiter's magnetic field at the completion of Juno's prime mission. *Journal of Geophysical Research: Planets*, *127*(2), e2021JE007055. https://doi.org/10.1029/2021JE007055

Damiano, P. A., Delamere, P. A., Stauffer, B., Ng, C.-S., & Johnson, J. R. (2019). Kinetic simulations of electron acceleration by dispersive scale Alfvén waves in Jupiter's magnetosphere. *Geophysical Research Letters*, *46*(6), 3043–3051. https://doi.org/10.1029/2018GL081219

Drell, S. D., Foley, H. M., & Ruderman, M. A. (1965). Drag and propulsion of large satellites in the ionosphere; An Alfvén propulsion engine in space. *Physical Review Letters*, *14*(6), 171–175. https://doi.org/10.1103/PhysRevLett.14.171

Drossart, P., Maillard, J., Caldwell, J., Kim, S., Watson, J., Majewski, W., et al. (1989). Detection of H3+ on Jupiter. *Nature*, *340*(6234), 539–541. https://doi.org/10.1038/340539a0

Gladstone, G. R., Stern, S. A., Slater, D. C., Versteeg, M., Davis, M. W., Retherford, K. D., et al. (2007). Jupiter's nightside airglow and aurora. *Science*, *318*(5848), 229–231. https://doi.org/10.1126/science.1147613

Gladstone, G. R., Waite, J. H., Grodent, D., Lewis, W. S., Crary, F. J., Elsner, R. F., et al. (2002). A pulsating auroral X-ray hot spot on Jupiter. *Nature*, *415*(6875), 1000–1003. https://doi.org/10.1038/4151000a

Grodent, D. (2015). A brief review of ultraviolet auroral emissions on giant planets. *Space Science Reviews*, *187*(1–4), 23–50. https://doi.org/10.1007/s11214-014-0052-8

Grodent, D., Gérard, J.-C., Gustin, J., Mauk, B. H., Connerney, J. E. P., & Clarke, J. T. (2006). Europa's FUV auroral tail on Jupiter. *Geophysical Research Letters*, *33*(6). https://doi.org/10.1029/2005GL025487

Grodent, D., Gérard, J.-C., Radioti, A., Bonfond, B., & Saglam, A. (2008). Jupiter's changing auroral location. *Journal of Geophysical Research*, *113*(A1). https://doi.org/10.1029/2007JA012601

Hess, S. L. G., Delamere, P., Dols, V., Bonfond, B., & Swift, D. (2010). Power transmission and particle acceleration along the Io flux tube. *Journal of Geophysical Research*, *115*(A6). https://doi.org/10.1029/2009JA014928

Hess, S. L. G., Pétin, A., Zarka, P., Bonfond, B., & Cecconi, B. (2010). Lead angles and emitting electron energies of Io-controlled decameter radio arcs. *Planetary and Space Science*, *58*(10), 1188–1198. https://doi.org/10.1016/j.pss.2010.04.011

Hill, T. (1979). Inertial limit on corotation. *Journal of Geophysical Research*, *84*(A11), 6554–6558. https://doi.org/10.1029/JA084iA11p06554

Hinton, P. C., Bagenal, F., & Bonfond, B. (2019). Alfvén wave propagation in the Io plasma torus. *Geophysical Research Letters*, *46*(3), 1242–1249. https://doi.org/10.1029/2018GL081472

Hue, V., Gladstone, G. R., Louis, C. K., Greathouse, T. K., Bonfond, B., Szalay, J. R., et al. (2023). The Io, Europa and Ganymede auroral footprints at Jupiter in the ultraviolet: Positions and equatorial lead angles. *Journal of Geophysical Research: Space Physics*, *128*(5), e2023JA031363. https://doi.org/10.1029/2023JA031363

Jones, S. T., & Su, Y.-J. (2008). Role of dispersive Alfvén waves in generating parallel electric fields along the Io-Jupiter fluxtube. *Journal of Geophysical Research*, *113*(A12). https://doi.org/10.1029/2008JA013512

Kedziora-Chudczer, L., Cotton, D. V., Kedziora, D. J., & Bailey, J. (2017). The 2 µm spectrum of the auroral emission in the polar regions of Jupiter. *Icarus*, *294*, 156–171. https://doi.org/10.1016/j.icarus.2017.04.029

Kita, H., Fujisawa, S., Tao, C., Kagitani, M., Sakanoi, T., & Kasaba, Y. (2018). Horizontal and vertical structures of Jovian infrared aurora: Observation using Subaru IRCS with adaptive optics. *Icarus*, *313*, 93–106. https://doi.org/10.1016/j.icarus.2018.05.002

Kivelson, M. G., Bagenal, F., Kurth, W. S., Neubauer, F. M., Paranicas, C., & Saur, J. (2004). Magnetospheric interactions with satellites. In F. Bagenal (Ed.), *Jupiter: The planet, satellites and magnetosphere* (Vol. 21, p. 513). Cambridge University Press.

Kurth, W. S., Imai, M., Hospodarsky, G. B., Gurnett, D. A., Louarn, P., Valek, P., et al. (2017). A new view of Jupiter's auroral radio spectrum. *Geophysical Research Letters*, *44*(14), 7114–7121. https://doi.org/10.1002/2017GL072889

McComas, D. J., Alexander, N., Allegrini, F., Bagenal, F., Beebe, C., Clark, G., et al. (2017). The Jovian auroral distributions experiment (JADE) on the Juno mission to Jupiter. *Space Science Reviews*, *213*(1), 547–643. https://doi.org/10.1007/s11214-013-9990-9

Miller, S., Tennyson, J., Geballe, T. R., & Stallard, T. (2020). Thirty years of H3+ astronomy. *Reviews of Modern Physics*, *92*(3), 035003. https://doi.org/10.1103/RevModPhys.92.035003

Moirano, A. (2023). Data for the research article: "The infrared footprint tracks of Io, Europa and Ganymede at Jupiter observed by Juno-JIRAM" [Dataset]. Zenodo. https://doi.org/10.5281/zenodo.10303022

Moirano, A., Gomez Casajus, L., Zannoni, M., Durante, D., & Tortora, P. (2021). Morphology of the Io plasma torus from Juno radio occultations. *Journal of Geophysical Research: Space Physics*, *126*(10), e2021JA029190. https://doi.org/10.1029/2021JA029190

Moirano, A., Mura, A., Adriani, A., Dols, V., Bonfond, B., Waite, J. H., et al. (2021). Morphology of the auroral tail of Io, Europa, and Ganymede from JIRAM L-band imager. *Journal of Geophysical Research: Space Physics*, *126*(9), e2021JA029450. https://doi.org/10.1029/2021JA029450

Moirano, A., Mura, A., Bonfond, B., Connerney, J. E. P., Dols, V., Grodent, D., et al. (2023). Variability of the auroral footprint of Io detected by Juno-JIRAM and modeling of the Io plasma torus. *Journal of Geophysical Research: Space Physics*, *128*(8), e2023JA031288. https://doi.org/10.1029/2023JA031288

Mura, A., Adriani, A., Altieri, F., Connerney, J. E. P., Bolton, S. J., Moriconi, M. L., et al. (2017). Infrared observations of Jovian aurora from Juno's first orbits: Main oval and satellite footprints: Jovian Aurora IR Observations from Juno. *Geophysical Research Letters*, *44*(11), 5308–5316. https://doi.org/10.1002/2017GL072954

Mura, A., Adriani, A., Connerney, J. E. P., Bolton, S., Altieri, F., Bagenal, F., et al. (2018). Juno observations of spot structures and a split tail in Io-induced aurorae on Jupiter. *Science*, *361*(6404), 774–777. https://doi.org/10.1126/science.aat1450

Natan, A. (2021). Fast 2D peak finder [Software]. MATLAB Central File Exchange. Retrieved from https://www.mathworks.com/matlabcentral/fileexchange/37388-fast-2d-peak-finder

Neubauer, F. (1980). Nonlinear standing Alfvén wave current system at Io: Theory. *Journal of Geophysical Research*, *85*(A3), 1171–1178. https://doi.org/10.1029/JA085iA03p01171

Phipps, P. H., Withers, P., Vogt, M. F., Buccino, D. R., Yang, Y., Parisi, M., et al. (2020). Where is the Io plasma torus? A comparison of observations by Juno radio occultations to predictions from Jovian magnetic field models. *Journal of Geophysical Research: Space Physics*, *125*(8). https://doi.org/10.1029/2019JA027633

Prangé, R., Rego, D., Southwood, D., Zarka, P., Miller, S., & Ip, W. (1996). Rapid energy dissipation and variability of the Io–Jupiter electro-dynamic circuit. *Nature*, *379*(6563), 323–325. https://doi.org/10.1038/379323a0

Promfu, T., Nichols, J. D., Wannawichian, S., Clarke, J. T., Vogt, M. F., & Bonfond, B. (2022). Ganymede's auroral footprint latitude: Comparison with magnetodisc model. *Journal of Geophysical Research: Space Physics*, *127*(12). e2022JA030712. https://doi.org/10.1029/2022JA030712

Saur, J. (2004). A model of Io's local electric field for a combined Alfvénic and unipolar inductor far-field coupling. *Journal of Geophysical Research*, *109*(A1). https://doi.org/10.1029/2002JA009354

Sulaiman, A. H., Hospodarsky, G. B., Elliott, S. S., Kurth, W. S., Gurnett, D. A., Imai, M., et al. (2020). Wave-particle interactions associated with Io's auroral footprint: Evidence of Alfvén, ion cyclotron, and whistler modes. *Geophysical Research Letters*, *47*(22). https://doi.org/10.1029/2020GL088432

Szalay, J. R., Allegrini, F., Bagenal, F., Bolton, S. J., Bonfond, B., Clark, G., et al. (2020a). Alfvénic acceleration sustains Ganymede's footprint tail aurora. *Geophysical Research Letters*, *47*(3). https://doi.org/10.1029/2019GL086527

Szalay, J. R., Allegrini, F., Bagenal, F., Bolton, S. J., Bonfond, B., Clark, G., et al. (2020b). A new framework to explain changes in Io's footprint tail electron fluxes. *Geophysical Research Letters*, *47*(18). https://doi.org/10.1029/2020GL089267

Tao, C., Badman, S. V., & Fujimoto, M. (2011). UV and IR auroral emission model for the outer planets: Jupiter and Saturn comparison. *Icarus*, *213*(2), 581–592. https://doi.org/10.1016/j.icarus.2011.04.001

Trafton, L., Carr, J., Lester, D., & Harvey, P. (1989). *Jupiter's aurora: Detection of quadrupole h2 emission* (p. 494). NASA Special Publication.

Wilson, R. J., Vogt, M. F., Provan, G., Kamran, A., James, M. K., Brennan, M., & Cowley, S. W. H. (2023). Internal and external Jovian magnetic fields: Community code to serve the magnetospheres of the outer planets community. *Space Science Reviews*, *219*(1), 15. https://doi.org/10.1007/s11214-023-00961-3